Mechanisms of vaccines against viral infections

Pardieck, I.N.

CHAPTER 7

A third vaccination with a single T cell epitope confers protection in a murine model of SARS-CoV-2 infection

Iris N. Pardieck, Tetje C. van der Sluis, Esmé T.I. van der Gracht, Dominique M.B. Veerkamp, Felix M. Behr, Suzanne van Duikeren, Guillaume Beyrend, Jasper Rip, Reza Nadafi, Elham Beyranvand Nejad, Nils Mülling, Dena J. Brasem, Marcel G.M. Camps, Sebenzile K. Myeni, Peter J. Bredenbeek, Marjolein Kikkert, Yeonsu Kim, Luka Cicin-Sain, Tamim Abdelaal, Klaas P.J.M. van Gisbergen, Kees L.M.C. Franken, Jan Wouter Drijfhout, Cornelis J.M. Melief, Gerben C.M. Zondag, Ferry Ossendorp, Ramon Arens

Nat Commun. 2022 Jul 8;13(1):3966.

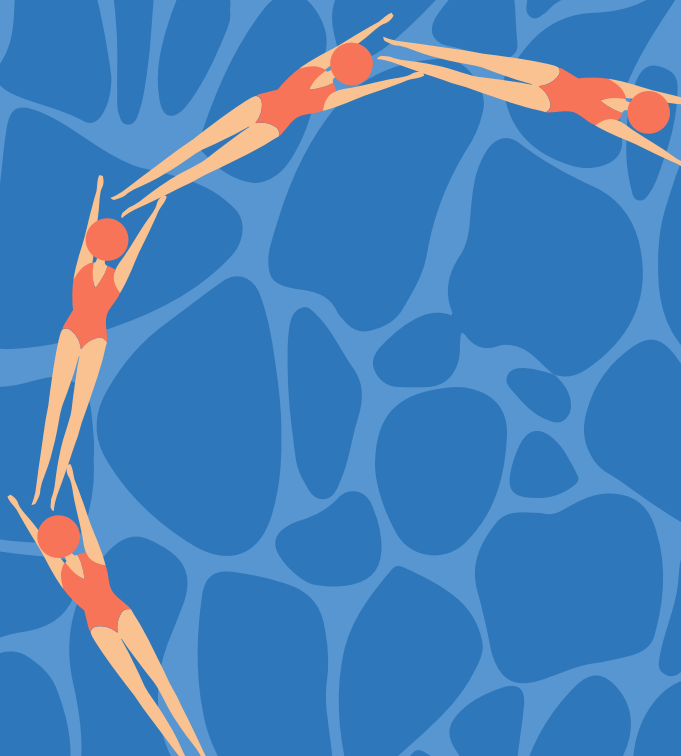

SUMMARY

A third dose with a single T cell epitope-vaccine promotes a strong increase in $CD8^+$ circulating effector-memory and tissue-resident memory T cells and fully protects against SARS-CoV-2 infection in absence of neutralizing antibodies.

ABSTRACT

Understanding the mechanisms and impact of booster vaccinations can facilitate decisions on vaccination programmes. This study shows that three doses of the same synthetic peptide vaccine eliciting an exclusive $CD8^+$ T cell response against one SARS-CoV-2 Spike epitope protects all mice against lethal SARS-CoV-2 infection in the K18-hACE2 transgenic mouse model in the absence of neutralizing antibodies, while only a second vaccination is insufficient to provide protection. The third vaccine dose of the single T cell epitope peptide results in superior generation of effector-memory T (T_{EM}) cells and tissue-resident memory T (T_{RM}) cells, and these tertiary vaccine-specific $CD8^+$ T cells are characterized by enhanced polyfunctional cytokine production. Moreover, fate mapping show that a substantial fraction of the tertiary $CD8^+$ T_{EM} cells develops from remigrated T_{RM} cells. Thus, repeated booster vaccinations quantitatively and qualitatively improve the $CD8^+$ T cell response leading to protection against otherwise lethal SARS-CoV-2 infection.

INTRODUCTION

The coronavirus disease 2019 (COVID-19) pandemic, caused by the β-coronavirus severe acute respiratory syndrome coronavirus 2 (SARS-CoV-2), remains a global health emergency. Vaccines eliciting neutralizing antibodies against the Spike protein of SARS-CoV-2 have shown high effectiveness (1, 2). However, the level of neutralizing antibodies declines after vaccination (3) and at-risk patient groups, including transplant recipients, individuals suffering from B cell leukemia, and auto-immune disease patients on selected immunosuppressive regimens (such as B cell depleting reagents), exhibit lower humoral and cellular immunity after vaccination (4-6). Moreover, the mutation rate of coronaviruses is substantial and certain mutations in the Spike protein of SARS-CoV-2 have emerged that can lead to a decline in neutralizing antibody-mediated protection (7, 8). In order to address this clinical problem, a third vaccination for solid organ transplant recipients is becoming the standard of care in more and more countries, and supplementary T cell-focused strategies have been suggested (9, 10).

While boosters with the current vaccines likely lead to the generation of enhanced levels of neutralizing antibodies, it is uncertain if this will improve protection in the aforementioned risk groups and provide protection against the emergence of novel SARS-related viruses. However, a third vaccination may also lead to enhanced T cell responses, which is expected to contribute to the control of SARS-CoV-2 infection as evidenced by their association to disease severity and protection in humans (11-16) and animal models (17, 18). Moreover, T cell-focused vaccines can be directed to more conserved regions of the coronavirus, which may lead to a broad T cell-based cross-protection against multiple coronavirus strains and likely independently expands the protection provided by antibodies. Such T cell-mediated protection is important given the potential emergence of similar viruses in the future that pose a significant threat to global public health. Previous studies showed that T cells can mediate protection by themselves against SARS-CoV-1 (19, 20) but whether T cell-eliciting vaccines can protect against SARS-CoV-2 is unclear. Here, we demonstrate that a peptide vaccine exclusively eliciting $CD8^+$ T cell responses against a single epitope present in the Spike protein delivers full protection against SARS-CoV-2, provided that the vaccine was administered in a double booster regimen, leading to the induction of high numbers of circulating and tissue-resident memory T (T_{RM}) cells. A third vaccination was especially critical to achieve cytokine polyfunctionality and induction of elevated T_{RM} cell numbers in the lungs and liver, and additionally fueled retrograde migration of T_{RM} cells into the circulation. Thus, booster vaccinations eliciting strong $CD8^+$ T cell responses are a promising strategy against coronavirus-mediated disease independent of neutralizing antibodies.

MATERIALS AND METHODS

Mice. Wild-type C57BL/6 mice were obtained from Charles River Laboratories, Jackson Laboratory or Janvier Labs. The K18-hACE2 transgenic mice, expressing the human ACE2 receptor (hACE2) under control of the cytokeratin 18 (K18) promoter (41), were obtained from the Jackson Laboratory (B6.Cg-Tg(K18-ACE2)2Prlmn/J), and bred in-house. The Hobit reporter × ROSA26-eYFP LT mice were previously described (32). At the start of the experiments, male and female mice were 6-8 weeks old. Animals were housed in individually ventilated cages under specific-pathogen free conditions at the animal facility at the Leiden University Medical Center (LUMC). All animal experiments were approved by the Animal Experiments Committee of LUMC and performed according to the recommendations and guidelines set by LUMC and by the Dutch Experiments on Animals Act.

Peptide and DNA-based vaccination. SARS-CoV-2 linear B cell epitopes, $Spike_{539-546}$-SLP, GP_{34-41}-SLP and $OVA_{257-264}$-SLP (aa sequences in Supplementary Table 2) were produced at the peptide facility of the LUMC. The purity of the synthesized peptide (75–90%) was determined by HPLC and the molecular weight by mass spectrometry. For the linear B cell epitope studies, mice were vaccinated subcutaneously (s.c.) at the tail base with 150 µg SLP + 20 µg CpG (ODN 1826, InvivoGen) dissolved in PBS and emulsified at a 1:1 ratio with Incomplete Freunds Adjuvant (Sigma Aldrich). For the $CD8^+$ T cell SLPs, mice were vaccinated s.c. at the tail base with 100 µg of the $Spike_{539-546}$, GP_{34-41} or $OVA_{257-264}$-SLP + 20 µg CpG (ODN 1826, InvivoGen) dissolved in PBS. Booster vaccinations were provided with 2 weeks interval. For DNA-based vaccination, a codon-optimized, synthetic gene encoding the Spike protein of SARS-CoV-2 was generated. Plasmids were propagated in *E. coli* cultures and purified using Nucleobond Xtra maxi EF columns (Macherey-Nagel) according to manufacturer's instructions. For vaccination, plasmids were column-purified twice, each time using a fresh column. Mice were intradermally vaccinated at the tail base with a total volume of 30 µL, containing 50 µg DNA in Tris-buffered saline (1 mM Tris, 0.9% NaCl). Booster vaccinations were provided with 3 weeks interval.

SARS-CoV-2 infection. Clinical isolate SARS-CoV-2/human/NLD/Leiden-0008/2020 (here named SARS-CoV-2) was obtained from a nasopharyngeal sample. The next-generation sequencing data of this virus isolate is available under GenBank accession number MT705206.1 and shows one mutation in the Leiden-0008 virus Spike protein compared to the Wuhan spike protein resulting in Asp>Gly substitution at position 614 (D614G). In addition, several non-silent (C12846U and C18928U) and silent mutations (C241U, C3037U, and C1448U) in other genes were found. Isolate Leiden-0008 was

propagated and titrated in Vero-E6 cells. K18-hACE2 transgenic mice were anaesthetized with isoflurane gas and intranasally infected with 5×10^3 plaque forming units (PFU) of SARS-CoV-2 in a total volume of 50 µl DMEM. Mouse weight and clinical discomfort were monitored daily. All experiments with SARS-CoV-2 were performed in the Biosafety Level 3 (BSL3) Laboratories at the Leiden University Medical Center.

Antigen-binding ELISA. ELISAs were performed to determine antibody titers in sera. Nunc ELISA plates were coated with 1 µg/ml Spike S1+S2ECD-His recombinant protein (SinoBiologicals) in ELISA coating buffer (Biolegend) overnight at 4°C. Plates were washed five times and blocked with 1% bovine serum albumin (BSA) in PBS with 0.05% Tween-20 for 1h at room temperature. Plates were washed and incubated with serial dilutions of mouse sera and incubated for 1h at room temperature. Plates were again washed and then incubated with 1:4000 dilution of horse radish peroxidase (HRP) conjugated anti-mouse IgG secondary antibody (SouthernBiotech, cat. 1030-05) and incubated for 1h at RT. To develop the plates, 50 µL of TMB 3,3=,5,5=tetramethylbenzidine) (Sigma-Aldrich) was added to each well and incubated for 5 minutes at room temperature. The reaction was stopped by the addition of 50 µL 1M H_2SO_4, and within 5 minutes the plates were measured with a microplate reader (model 680; Bio-Rad) at 450 nm

Virus neutralization assay (VNA). Serum was heat-inactivated for 0.5h at 56 ˚C, two-fold serially diluted and incubated with 100 PFU/100µl of SARS-CoV-2 Zagreb isolate (hCoV-19/Croatia/ZG-297-20/2020, GISAID database ID: EPI_ISL_451934) for 1 h at room temperature. Thereupon, 2×10^4 Vero-E6 (ATCC CRL-1586) cells that were seeded in 96-well plates were inoculated with serum and virus. Following 1 h incubation at 37 °C and 5% CO_2, the inoculum was removed, and 1.5% methylcellulose overlay was added. Infected cells were incubated for 3 days at 37 °C and 5% CO_2, prior to crystal violet staining and plaque counting.

Single-cell preparations. Peripheral blood was collected from the tail vein. Splenocytes were obtained by mincing the tissue through cell strainers. Blood cells and splenocytes were depleted of erythrocytes using ammonium chloride lysis buffer. To remove remaining circulating blood cells from the liver and lungs, mice were perfused with 20 ml PBS containing 2 mM EDTA. Next, liver and lungs were cut into small pieces using surgical knives, and the tissue was resuspended in 3.5 ml or 1 ml, respectively, of IMDM containing 250 U/ml collagenase type 1-A (C2674, Sigma) and 20 µg/ml DNase I (D5025, Sigma). After incubation with collagenase/DNase for 25 minutes at 37°C, liver and lung tissue was dissociated into single-cell suspensions using 70 µm cell strainers, and subsequently lymphocytes were isolated using a Percoll (GE Healthcare) gradient.

Flow cytometry. Following resuspension in staining buffer (PBS +1% FCS) the cells were incubated with fluorescently labelled antibodies to: CD3 (clone 145-2C11, BD Biosciences; clone 17A2, ThermoFisher), CD4 (clone RM4-5, BioLegend; clone GK1.5, ThermoFisher), CD8 (clone 53-6.7, BioLegend), KLRG1 (clone 2F1, ThermoFisher), CD44 (clone IM7, BioLegend), CD62L (clone MEL-14, BioLegend), CD69 (clone H1.2F3, BD Biosciences), CX3CR1 (clone SA011F11, BioLegend), Ly6C (clone HK1.4, BioLegend), Eomes (clone Dan11mag, Invitrogen), TNF (clone MP6-XT22, BioLegend), IFN-γ (clone XMG1.2, ThermoFisher), PD-1 (clone J43, BD Biosciences), Ki-67 (clone 16A8, BioLegend), CXCR3 (clone CXCR3-173, BioLegend), CD19 (clone 6D5, BioLegend), CD43 (clone 1B11, BioLegend), TCF1 (clone S33-966, BD Biosciences). Zombie Aqua (BioLegend) staining was used to exclude dead cells. To stain EOMES and TCF1, cells were fixed for 30 min using the Fixation/Permeabilization concentrate (Invitrogen, FOXP3/Transcription factor Staining buffer set), diluted 1:6 in eBioscience™ Fixation/Perm diluent Following 2 washes in Permeabilization Buffer (diluted according to manufactures instructions) anti-TCF1 and anti-EOMES were diluted in Permeabilization Buffer and incubated for 1 h. Following a washing step in staining buffer the cells were ready for analysis. Glucose uptake was measured by the uptake of glucose analogue 2-(N-(7-nitrobenz-2-oxa-1,3-diazol-4-yl)amino)-2-deoxyglucose (2-NBDG, Life Technologies). Cell surface and intracellular cytokine stainings of splenocytes and blood lymphocytes were performed as described (42). PADRE-specific $CD4^+$ T cells were quantified using an MHC class II tetramer for the epitope (AKFVAAWTLKAA) (NIH Tetramer Core Facility). $Spike_{539-546}$-specific, GP_{34-41}-specific or $OVA_{257-264}$-specific $CD8^+$ T cells were quantified using MHC class I tetramers generated in-house. For examination of intracellular cytokine production, single cell suspensions were stimulated with short peptides for 5 h in the presence of brefeldin A or with long peptides for 8 h of which the last 6 h in presence of brefeldin A (Golgiplug; BD Pharmingen). Flow cytometric acquisition was performed on a BD Fortessa flow cytometer (BD Biosciences) or Aurora Cytek spectral analyzer, and samples were analyzed using FlowJo software (TreeStar) and OMIQ data analysis software (Gating strategy shown in **Supplementary Figure 5**).

Adoptive T cell transfers. Spleens of OT-I Hobit reporter × ROSA26-eYFP LT mice were isolated and subsequently OT-I $CD8^+$ T cells were isolated by negative selection using MicroBeads (130-104-075, Miltenyi Biotec) according to the manufacturer's protocol. Splenic OT-I $CD8^+$ T cells were adoptively transferred via retro-orbital injection into naïve mice.

Statistical analysis. Statistical analyses were performed using Cytofast or GraphPad Prism (La Jolla, CA, Unites States). One-way ANOVA and log-rank (Mantel-Cox) survival

test were used for statistical analysis. All P values were two-sided, and $P < 0.05$ was considered statistically significant.

RESULTS

Vaccines eliciting antibodies against confirmational proteins but not linear B cell epitopes are neutralizing and effective against SARS-CoV-2 infection

Single B and T cell epitope vaccines can provide effective approaches against a variety of pathogens and malignancies (21-24). To investigate the efficacy of linear B cell epitope vaccines against SARS-CoV-2 infection, we selected five different linear epitopes present in the Spike protein that were considered to potentially elicit protective antibodies (25-27). To test their immunogenicity, C57BL/6 mice were vaccinated with synthetic long peptide (SLP)-based vaccines each containing a single B cell epitope. After three vaccinations, however, these SLP vaccines did not elicit Spike-specific antibody responses (**Supplementary Figure 1A**). To improve this synthetic vaccine, we tested the particular influence of the adjuvants and of CD4 help on the specific antibody induction of the B cell-SLP vaccines. To this end, the SLP-based vaccines were provided coupled with the universal helper epitope PADRE adjuvanted with CpG and Incomplete Freund's Adjuvant (IFA). The combination of these adjuvants acted synergistically to elicit high levels of antibodies against the Spike protein (**Figure 1A**). This synergistic effect correlated with a higher induction of PADRE-specific $CD4^+$ T cell responses (**Figure 1B, 1C**). Coupling of the PADRE epitope to the linear B cell epitopes also contributed to the improvement of the Spike-specific IgG antibody response, instead of combining the linear B cell epitopes and PADRE epitope in a single vaccine (**Figure 1D, Supplementary Figure 1B**). Moreover, depletion of $CD4^+$ T cells during the vaccination period resulted in a decreased spike-specific antibody response (**Supplementary Figure 1C**), highlighting the need for $CD4^+$ T cells for an optimal IgG response. $CD8^+$ T cell responses were not induced by the B cell-SLP vaccines (**Supplementary Figure 1D**).

To determine whether immunization with optimized linear B cell epitope vaccines enables protective immune responses against SARS-CoV-2, we used transgenic mice expressing the human angiotensin I-converting enzyme 2 (ACE2) receptor under the regulation of the cytokeratin 18 (K18) promoter, which develop severe lung disease in response to SARS-CoV-2 infection (28). The K18-hACE2 mice were vaccinated three times with a two week interval with either one CpG/IFA adjuvanted PADRE-coupled B cell-SLP vaccine or a combination of the five different B cell-SLP vaccines. Spike-

specific IgG antibody responses were elicited and reached high titers after the third (3rd) vaccination (**Figure 1E**). Four weeks after the third vaccination, the K18-hACE2 mice were challenged intranasally with a lethal dose of SARS-CoV-2 and body weight was measured daily as a parameter of disease. Both unvaccinated mice and mice that were vaccinated three times with the B cell-SLPs succumbed to SARS-CoV-2 infection (**Figure 1F, 1G**), showing that SLP vaccination with these linear B cell epitopes was not able to protect against SARS-CoV-2 infection. This inability of protection correlated with the incapability of antibodies to neutralize virus cell entry (**Figure 1H**). In contrast, a DNA vaccine encoding the entire Spike protein fully protected K18-hACE2 transgenic mice from SARS-CoV-2 infection, and this correlated with the ability to elicit neutralizing Spike-specific antibodies (**Figure 1I**-**1L**). In addition, this DNA vaccine also induced a Spike-specific $CD4^+$ and $CD8^+$ T cell response (**Figure 1M, Supplementary Figure 1E**). The response against an immunodominant $CD8^+$ T cell epitope present in the Spike protein of SARS-CoV-1 and SARS-CoV-2 (29) increased upon the 2nd but not the 3rd vaccination, and was characterized by an increased expression of the activation-associated NK cell receptor KLRG1 (**Figure 1M, 1N**). Overall, these results indicate that antibody responses to these single linear B cell epitopes are inferior for the induction of neutralizing antibodies, although we cannot exclude the possibility that single linear B cell epitopes exist that can elicit neutralizing antibodies. Nevertheless, antibody responses induced by vaccine platforms encoding properly folded proteins presenting conformational B cell epitopes are able to generate neutralizing antibodies and provide protection against SARS-CoV-2 infection.

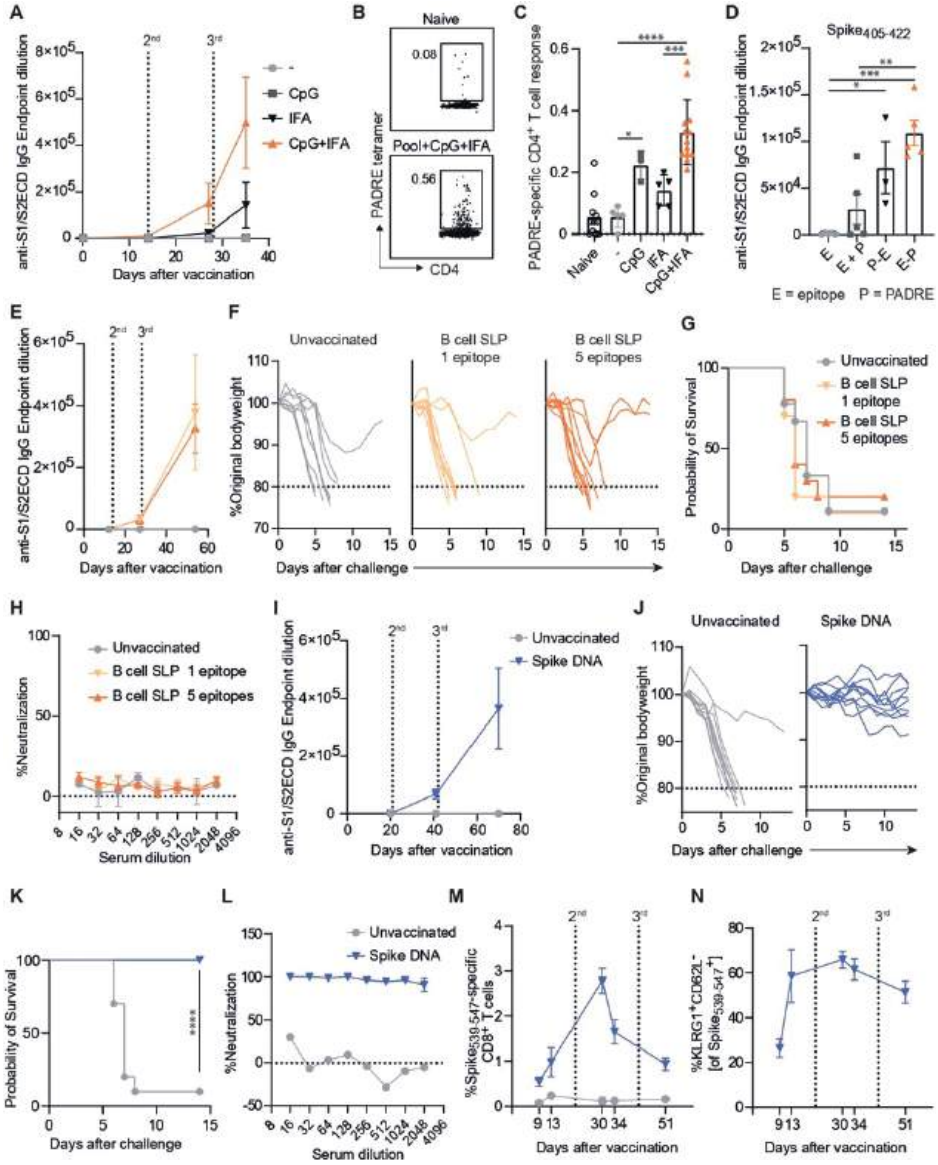

Figure 1. Vaccines eliciting antibodies against confirmational proteins but not linear B cell epitopes are neutralizing and effective against SARS-CoV-2 infection. (A) C57BL/6 mice were vaccinated subcutaneously (s.c.) on day 0, 14 and 28 with synthetic long peptides (SLPs) consisting of PADRE-coupled linear B cell epitopes (E-P) adjuvanted or not with CpG and/or Inactivated Freund's Adjuvant (IFA). Spike-specific IgG kinetics in blood. **(B)** Representative flow cytometry plots of PADRE-specific CD4⁺ T cells on day 21 after vaccination. **(C)** PADRE-specific CD4⁺ T cell response on day 21 after vaccination as described in (A) (n=3-13). **(D)** C57BL/6 mice were vaccinated as described in (A) with SLPs consisting of epitopes (E) coupled to PADRE (E-P, P-E), or equimolar SLP controls containing the epitope alone (E), or the epitope with uncoupled PADRE (E + P) adjuvanted with CpG and IFA. Endpoint dilutions of Spike-specific IgG in blood at day 42 after vaccination with $Spike_{405-422}$-SLP are shown (n=3- >

> 5). **(E-H)** K18-hACE2 transgenic mice were vaccinated on day 0, 14 and 28 with one or five SLP vaccines containing a PADRE-coupled linear B cell epitope adjuvanted with CpG and IFA. Four weeks after the final vaccination, mice were intranasally infected with SARS-CoV-2. **(E)** Spike-specific IgG kinetics in blood. **(F)** Weight loss kinetics after SARS-CoV-2 challenge. **(G)** Survival graph after SARS-CoV-2 challenge. Significance was determined by a log-rank test and corrected for multiple comparisons (n=9-10). **(H)** SARS-CoV-2 neutralizing capacity by antibodies after B cell-SLP vaccination on day 42 measured by a WT virus neutralization assay (VNA). **(I-N)** K18-hACE2 mice were vaccinated intradermally on day 0, 21 and 42 with a Spike-encoding DNA vaccine. Spike-specific IgG **(I)** and weight loss kinetics **(J)** after SARS-CoV-2 challenge. **(K)** Survival graph after SARS-CoV-2 challenge. Significance was determined by a log-rank test (n=10). **(L)** SARS-CoV-2 neutralizing capacity by antibodies after Spike DNA vaccination on day 55 measured a VNA. **(M)** Kinetics of $Spike_{539\text{-}546}$-specific $CD8^+$ T cells in blood. **(N)** Kinetics of $KLRG1^+CD62L^-$ expression on $Spike539_{\text{-}546}$-specific $CD8^+$ T cells in blood. Data is represented as mean ± SEM. In (C) and (D) one-way ANOVA with repeated measurements was performed to determine significance. *P<0.05, **P<0.01, ***P<0.001, ****P<0.0001.

A third vaccination with a peptide harboring a single T cell epitope protects against SARS-CoV-2 challenge

To determine whether an immune response induced by a single $CD8^+$ T cell epitope vaccine was able to protect against SARS-CoV-2 infection, K18-hACE2 transgenic mice were vaccinated once, twice or three times with an SLP encoding an immunodominant $CD8^+$ T cell epitope present in the Spike protein of SARS-CoV-1 and SARS-CoV-2 (29). Five weeks after the final vaccination, mice were intranasally challenged with a lethal dose of SARS-CoV-2 (**Figure 2A**). SLP vaccination induced a $Spike_{539\text{-}546}$-specific $CD8^+$ T cell response in all mice, which increased with each booster immunization and remained elevated after contraction (**Figure 2B-D**). $CD4^+$ T cell responses and spike-specific antibodies were not induced (**Supplementary Figure 1F, 1G**). Whereas 75% of the non-vaccinated mice succumbed to SARS-CoV-2 challenge, 66% and 50% of the mice that received one or two vaccinations, respectively, succumbed. Strikingly, all mice that received a third vaccine dose recovered from the SARS-CoV-2 challenge despite initial weight loss (**Figure 2E, 2F**). Thus, a third vaccination with an SLP containing a single $CD8^+$ T cell epitope protects against lethal SARS-CoV-2 infection.

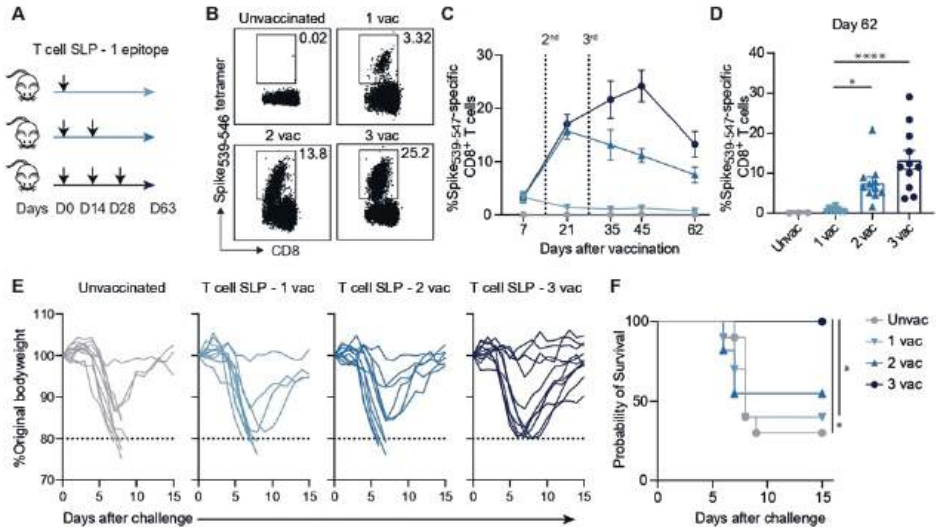

Figure 2. A third vaccination with a single T cell epitope protects against SARS-CoV-2 challenge. **(A)** K18-hACE2 transgenic mice were vaccinated subcutaneously on day 0 (1st vaccination), day 14 (2nd vaccination) and day 28 (3rd vaccination) with the $Spike_{539\text{-}546}$-SLP vaccine adjuvanted with CpG. The $Spike_{539\text{-}546}$-specific $CD8^+$ T cell response was determined in blood in time. Five weeks after the final vaccination, mice were intranasally infected with 5000 PFU of SARS-CoV-2, and monitored for weight loss and signs of clinical discomfort. **(B)** Representative flow cytometry plots of $Spike_{539\text{-}546}$-specific $CD8^+$ T cells determined in the blood circulation at day 45 by MHC class I tetramer staining. **(C)** $Spike_{539\text{-}546}$-specific $CD8^+$ T cell kinetics in blood at indicated days after vaccination. Data is represented as mean ± SEM. **(D)** $Spike_{539\text{-}546}$-specific $CD8^+$ T cells in blood at day 62 after vaccination. Bar graphs represent means ± SEM. Symbols represent individual mice. One-way ANOVA with repeated measurements was performed to determine statistical significance (n=10-11). **(E)** Weight loss kinetics in time of SARS-CoV-2 challenged K18-hACE2 transgenic mice after T cell epitope SLP vaccination. **(F)** Survival graph of SARS-CoV-2 challenged K18-hACE2 transgenic mice after T cell SLP vaccination. Significance was determined by a log-rank test and corrected for multiple comparisons (n=10-11). *P<0.05, ****P<0.0001.

A third vaccination with a single T cell epitope augments effector-memory and tissue-resident memory $CD8^+$ T cell formation

Next, we aimed to determine the impact and underlying mechanisms of sequential SLP vaccinations on the memory differentiation of the elicited antigen-specific $CD8^+$ T cells. Three times vaccinated mice had 4-fold higher frequencies of circulating ($CD69^-$) $Spike_{539\text{-}546}$-specific $CD8^+$ T cells in the spleen compared to two times vaccinated mice, and 16-fold higher frequencies compared to once vaccinated mice (**Figure 3A**). In the liver, the third vaccination resulted in a notably higher $Spike_{539\text{-}546}$-specific $CD8^+$ T cell response compared to the single (120-fold increase) or double vaccination (34-fold increase), and this difference was principally due to an increment of the $CD69^+$ T_{RM} cells. In the lungs, the third vaccination resulted in an 20-fold and 4-fold enhancement of $Spike_{539\text{-}546}$-specific $CD69^+$ T_{RM} cells compared to single and double vaccination, respectively. Circulating ($CD69^-$) $Spike_{539\text{-}546}$-specific T cells in the lungs were 15-fold

and 5-fold increased after the third vaccination compared to the first (1st) and second (2nd) vaccination, respectively (**Figure 3A, Supplementary Figure 2A**). To investigate the effector potential of these Spike$_{539-546}$-specific CD8$^+$ T cells, the polyfunctional cytokine production capacity of the vaccine-specific CD8$^+$ T cells was determined. The increment in frequency of the Spike$_{539-546}$-specific CD8$^+$ T cells after the 2nd and 3rd vaccination coincided with an increase in polyfunctional CD8$^+$ T cells (IFN-γ$^+$TNF$^+$, IFN-γ$^+$TNF$^+$IL-2$^+$) in spleen, liver and lungs (**Figure 3B**). Thus, sequential booster vaccinations elicits significant and durable expansion of cytokine polyfunctional cytokine-producing CD8$^+$ T cells.

Next, we investigated the effect of booster vaccination on the differentiation status of the elicited Spike$_{539-546}$-CD8$^+$ T cells. Analysis of these cells in the blood circulation using t-distributed stochastic neighbor embedding (tSNE) algorithms highlighted that the memory phenotype of the vaccine-specific CD8$^+$ T cells in blood was skewed towards an effector-memory like state (CD62L$^-$KLRG1$^+$Ly6C$^+$CX3CR1$^+$) by one booster vaccination, and that the 2nd booster vaccination (3rd vaccination) enforced this phenotype slightly further (**Figure 3C, D**). Moreover, in the tissues, booster vaccination also resulted in substantial alterations in the differentiation state and subset formation of the vaccine-elicited CD8$^+$ T cells. The Spike$_{539-546}$-specific CD8$^+$ T cells in the spleen mainly differentiated into CD62L$^-$KLRG1$^+$Ly6C$^+$CX3CR1$^+$ cells after the first booster (**Figure 3E, F**). These effector-memory-like cells were also present in the lungs, while in the liver, the large majority of the infiltrated cells were tissue-resident (CD69$^+$) and lacked expression of CX3CR1 and KLRG1 (**Figure 3E**). Uptake of the glucose analog 2-(N-(7-nitrobenz-2-oxa-1,3-diazol-4-yl)amino)-2-deoxyglucose (2-NBDG) (**Figure 3F**) was reduced following the first booster vaccination, indicating induction of a different metabolic efficiency after booster vaccination. Thus, while primarily the 2nd vaccination had a profound system-wide impact on the phenotype of the vaccine-induced CD8$^+$ T cells, the 3rd vaccination enhanced their numbers.

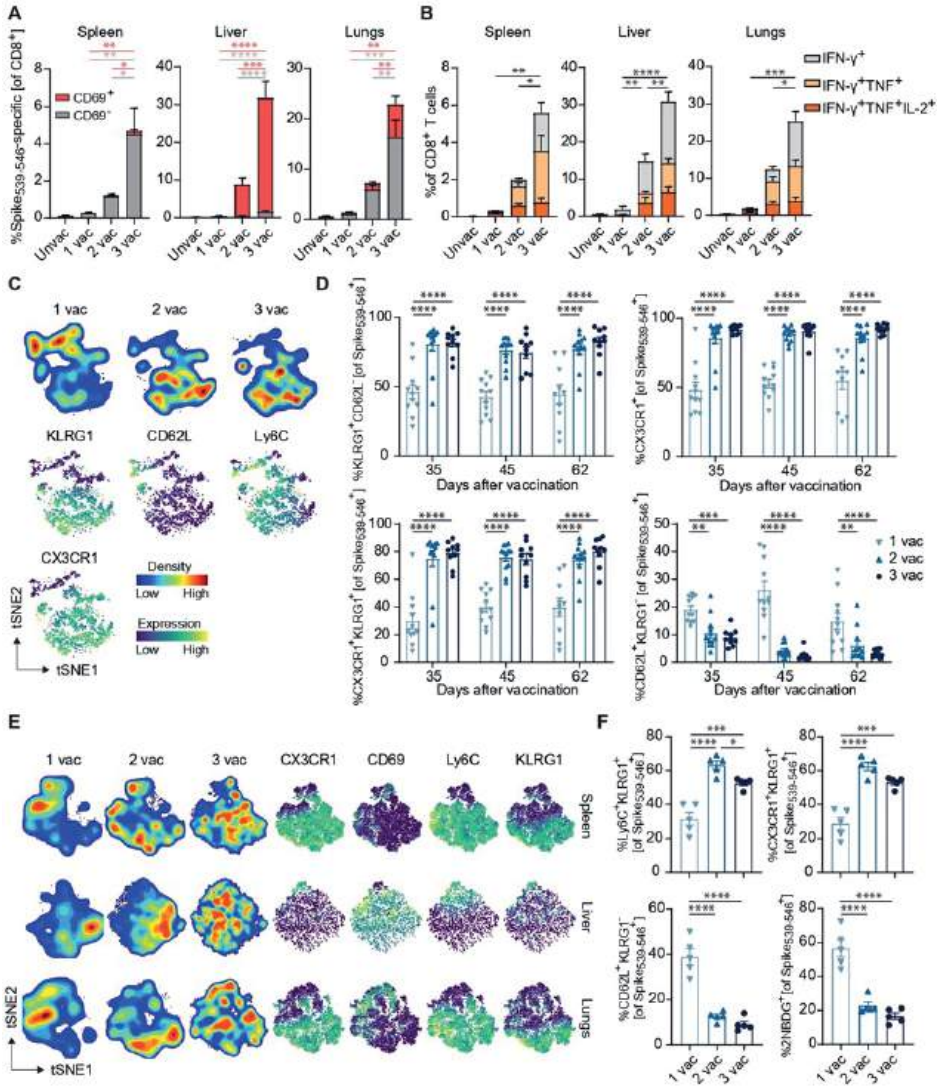

Figure 3. A third vaccination with a single T cell epitope augments effector-memory and tissue-resident memory CD8⁺ T cell formation. (A) Frequencies of CD69⁺ and CD69⁻ Spike$_{539-546}$-specific CD8⁺ T cells in the CD8⁺ T cell population in the spleen, liver and lungs at day 70 after 1, 2 or 3 SLP vaccinations. Bar graphs represent means ± SEM (n=5). One-way ANOVA with repeated measurements was performed to determine statistical significance. **(B)** Intracellular cytokine production of CD8⁺ T cells upon stimulation with the Spike$_{539-546}$ peptide epitope in different tissues on day 70 after SLP vaccination. Data is represented as mean ± SEM. One-way ANOVA with repeated measurements was performed to determine statistical significance (n=5). **(C)** tSNE maps describing the local probability density of Spike$_{539-546}$-specific CD8⁺ T cells stained for KLRG1, CD62L, Ly6C and CX3CR1 at day 62 after 1, 2 and 3 vaccinations. **(D)** Frequencies of KLRG1⁺CD62L⁻, CX3CR1⁺, CX3CR1⁺KLRG1⁺ and CD62L⁺KLRG1⁻ Spike$_{539-546}$-specific CD8⁺ T cells in blood in time. Bar graphs represent means ± SEM. Symbols represent individual mice. Two-way ANOVA with repeated measurements was performed to determine significance (n=10-12). **(E)** (Left) tSNE maps describing the local probability density of Spike$_{539-546}$-specific CD8⁺ T cells in spleen, >

> liver and lungs stained at day 69 after 1, 2 and 3 vaccinations with a flow cytometry panel for CD69, CD62L, CD44, Ly6C, KLRG1 and CX3CR1. (Right) marker expression for CX3CR1, CD69, Ly6C and KLRG1. **(F)** Cell surface marker (Ly6C$^+$KLRG1$^+$, CX3CR1$^+$KLRG1$^+$ and CD62L$^+$KLRG1$^-$) expression and percentage of the glucose analog 2-(N-(7-nitrobenz-2-oxa-1,3-diazol-4-yl)amino)-2-deoxyglucose (2NBDG) uptake of Spike$_{539\text{-}546}$-specific CD8$^+$ T cells at day 69 in spleen after 1, 2 or 3 vaccinations. One-way ANOVA with repeated measurements was performed to determine statistical significance (n=5). *P<0.05, **P<0.01, ***P<0.001, ****P<0.0001.

Progressive differentiation of vaccine-specific CD8$^+$ T cells after booster vaccination

To gain further insight into the differentiation of the vaccine-specific CD8$^+$ T cells upon sequential vaccination, we studied these cells in-depth using detailed single-cell high dimensional clustering analysis and trajectory inference with an antibody panel targeting multiple markers of cellular activation and differentiation. Visualization based on the cluster distribution of the splenic Spike$_{539\text{-}546}$-specific CD8$^+$ T cells indicated that the cells after the 1st vaccination were disparate from the 2nd and 3rd vaccination, while the 2nd and 3rd vaccination were largely overlapping (**Figure 4A**). Strikingly, and consistent with the aforementioned data, a large KLRG1$^+$ cluster (cluster #3) co-expressing Ly6C and lacking CD62L, was more profoundly present in the 2nd and 3rd vaccination group (**Figure 4A-D**). This cluster of cells also expressed CD44 and the cell proliferation marker Ki-67, but lacked expression of EOMES, TCF1, CXCR3, the activation-associated CD43^{1B11} isoform, and PD-1. Cluster #2, which had a similar expression except for KLRG1, was also increased in the 2nd and 3rd vaccination group compared to the 1st vaccination group (**Figure 4B, 4E**). Other significantly different clusters, which were relatively reduced after the 2nd and 3rd vaccination compared to the 1st vaccination, were characterized by either high levels of CD62L and TCF1, and lacking markers such as KLRG1 and CD44 (cluster #1) or expressed intermediate differentiation phenotypes (cluster #7: CD44$^+$ Ki-67$^+$Ly6C$^+$EOMES$^+$TCF1$^+$CXCR3$^+$PD-1$^+$KLRG1$^-$CD62L$^+$, cluster #6: CD44$^+$Ki-67$^+$Ly6C$^+$EOMES$^-$TCF1$^-$CXCR3^{int}PD-1$^-$KLRG1$^-$CD62L$^-$, and cluster #8: CD44$^+$Ki-67$^+$Ly6C$^+$EOMES$^+$TCF1$^+$CXCR3$^+$PD-1$^-$KLRG1$^-$CD62L$^-$ (**Figure 4B, 4D, 4E**). The single-cell trajectory algorithm Wanderlust (30) predicted that the developmental path progressed from the CD62L$^+$CD44$^-$TCF1$^+$ subset to transitional subsets harboring markers that were upregulated and retained (CD44, Ki-67 and Ly6C) or are eventually downregulated (EOMES, CXCR3, CD43^{1B11}) (**Figure 4A, 4F, 4G**). The initially expressed CD62L and TCF1 were downregulated whereas KLRG1 expression was acquired at a late-stage indicating a progressive effector-memory T (T_{EM}) cell differentiation program after booster vaccination (**Figure 4F, 4G**).

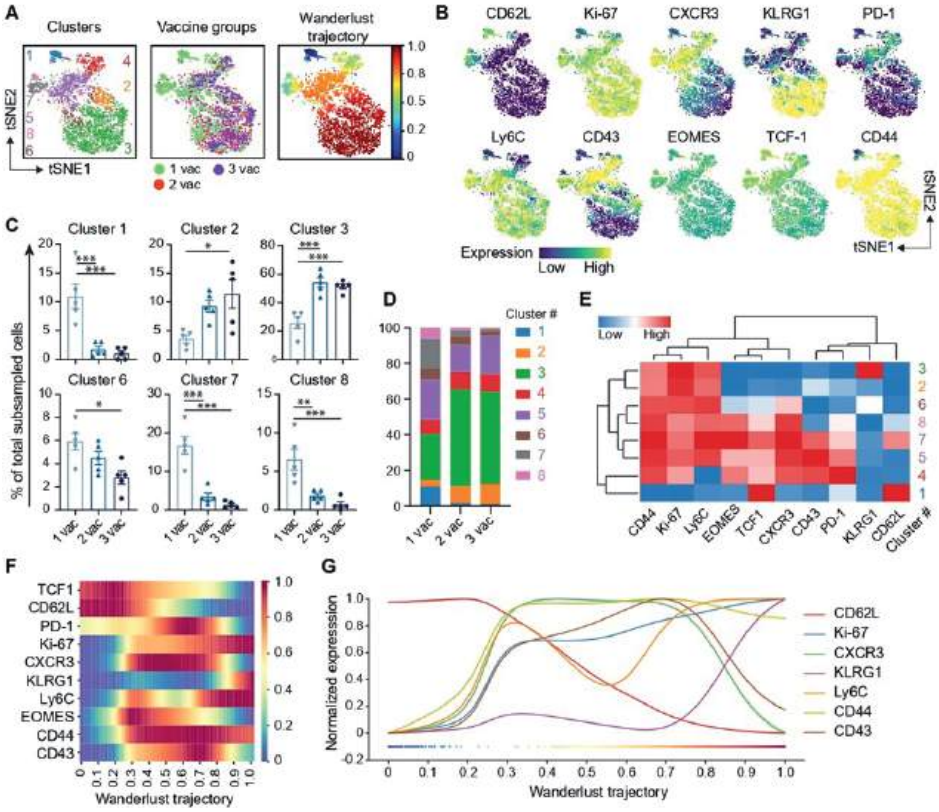

Figure 4. Progressive differentiation of vaccine-specific CD8⁺ T cells after booster vaccination. C57BL/6 mice were vaccinated subcutaneously on day 0 (1st vaccination), day 14 (2nd vaccination) and day 28 (3rd vaccination) with the Spike$_{539-546}$-SLP vaccine adjuvanted with CpG and sacrificed on day 69. **(A)** Following tSNE analysis downsampling, FlowSOM consensus metaclustering with 8 clusters as well as Wanderlust trajectory analysis was performed on 200 live CD3⁺CD8⁺CD4⁻CD19⁻ Spike$_{539-546}$ tetramer⁺ cells harvested from the spleen. Overlay of the 8 FlowSOM clusters (left), vaccination status (middle) and Wanderlust trajectory (right) (color indication: blue, beginning/early; red, end/late) on the tSNE-map. **(B)** Expression intensity of cell surface markers (color indication: blue, low expression; yellow, high expression) **(C)** Significant clusters were selected and are shown in bar graphs. Bar graphs represent means ± SEM. Symbols represent individual mice. One-way ANOVA with repeated measurements was performed to determine statistical significance (n=5). **(D)** Stacked bar graph of all 8 FlowSOM clusters per vaccination group, colors match (A). **(E)** Hierarchically clustered heatmap of phenotypes of the clusters shown in (A) – the indicated marker expression is shown per cluster as z-Score of median signal intensity per channel; blue, low expression; red, high expression. **(F)** Each of the markers used for embedding in figure (A-C) are displayed according to Wanderlust trajectory progression. **(G)** Selected markers are displayed according to Wanderlust trajectory progression.

Vaccine-specific conditions drive the differentiation of elicited CD8$^+$ T cells

To examine whether vaccine-specific conditions or the epitope itself influence the differentiation of the elicited CD8$^+$ T cells, we vaccinated mice with SLP vaccines containing the model antigen GP_{34-41} derived from lymphocytic choriomeningitis virus (LCMV) in a similar manner (**Supplementary Figure 2A**). As observed with the $Spike_{539-546}$-SLP immunization, each subsequent vaccination with GP_{34-41}-SLP, increased the magnitude of the vaccine-specific CD8$^+$ T cell response, and this response remained higher after contraction (**Supplementary Figure 2B-D**). Moreover, also the GP_{34-41}-specific CD8$^+$ T cells in the spleen, liver and lungs where significantly increased upon each vaccination. In the spleen this was caused by an increment of the circulating GP_{34-41}-specific CD8$^+$ T cells, in the liver by the CD69$^+$ GP_{34-41}-specific CD8$^+$ T_{RM} cells and in the lungs by an increase in both the circulating as well as the tissue-resident T cells (**Supplementary Figure 2E**). In addition, these increments were also reflected by increased polyfunctional cytokine producing GP_{34-41}-specific CD8$^+$ T cells in the spleen, liver and lungs (**Supplementary Figure 2F**). Analysis of the differentiation status of the GP_{34-41}-specific CD8$^+$ T cells in the blood circulation using tSNE algorithms also showed differentiation into an effector-memory like state (CD62L$^-$KLRG1$^+$Ly6C$^+$CX3CR1$^+$) after the 2nd vaccination, which was further manifested after the 3rd vaccination (**Supplementary Figure 2G-2J**). In addition, high-dimensional clustering analysis of the splenic GP_{34-41}-specific CD8$^+$ T cells after booster vaccination showed a similar pattern: a large KLRG1$^+$Ly6C$^+$Ki-67$^+$ cluster profoundly present in the 2nd and 3rd vaccination group and less differentiated clusters (CD62L$^+$TCF1$^+$KLRG1$^-$) that were relatively more abundant after the 1st vaccination (**Supplementary Figure 3A-D**).

Further insight into the phenotype of the vaccine-specific CD8$^+$ T cells upon sequential vaccination, using single-cell high dimensional mass cytometry with a panel of antibodies targeting markers of cellular activation and differentiation (31) (**Supplementary Figure 4A, Supplementary Table 1**), confirmed the disparate phenotype after the 1st vaccination compared to the 2nd and 3rd vaccination (**Supplementary Figure 4B**). Principal component analysis (PCA) based on the cluster frequencies of the GP_{34-41}-specific memory CD8$^+$ T cells in the spleen, liver and lungs confirmed the clear distinction between clusters present in one-time vaccinated *versus* clusters in two or three times vaccinated mice (**Supplementary Figure 4C**). In addition, dual tSNE analysis on all samples of the GP_{34-41}-specific CD8$^+$ T cells, visualizing the segregation based on vaccination-associated patterns, corroborated that the 2nd and 3rd vaccination-specific phenotypes had considerable overlaps (**Supplementary Figure 4D**). A low Jensen-Shannon (JS) divergence distance was calculated when comparing antigen-specific CD8$^+$ T cells induced upon 2nd and 3rd vaccinations, indicating a high similarity between

cells induced by these vaccinations, whereas a higher JS distance was apparent when comparing 1st to 2nd vaccinations or 1st to 3rd vaccinations (**Supplementary Figure 4E**). Visualization and quantification of the particular marker expression on the GP_{34-41}-specific $CD8^+$ T cell population indicated that in the spleen and lungs, the percentage $CD69^-CD62L^-$ T_{EM}-like cells expressing high levels of KLRG1, Ly6C and CX3CR1, and moderate expression of NKG2A, Sca-1 and the ectonucleotidase CD39 associated to the 2nd and 3rd vaccination, while the $CD69^-CD62L^+$ subsets related to single-dose vaccination (**Supplementary Figure 4F-H**). The phenotype of $CD69^+$ GP_{34-41}-specific $CD8^+$ T_{RM} cells in the liver was slightly affected upon the 2nd boosting, and resulted in reduction of $CD11c^+CD122^+PD\text{-}1^-$ T_{RM} cells and an increase in $CD11c^+CD122^-PD\text{-}1^+$ T_{RM} cells (**Supplementary Figure 4H**). Based on the induction of a highly similar phenotype by the $Spike_{539-546}$-SLP and GP_{34-41}-SLP vaccines, we conclude that the differentiation of the vaccine-elicited $CD8^+$ T cells depends on (repeated) vaccine-specific conditions rather than the antigens itself.

A third vaccination triggers the remigration of T_{RM} cells into the circulation

To fate map the T_{RM} cell progeny upon booster vaccination, we used a reporter system based on the T_{RM}-restricted transcription factor Hobit to evaluate the development of the T_{RM} cells (32). Here, Hobit lineage tracer (LT) mice, which were generated by crossing CD45.1 Hobit reporter OT-I mice with ROSA26-eYFP mice, were used. $CD8^+$ T cells in these mice recognize the epitope SIINFEKL ($OVA_{257-264}$) and report active Hobit expression (by tdTomato expression) and previous Hobit expression (by YFP expression), which allows the detection of ex-Hobit$^+$ cells (ex-T_{RM}; $tdTomato^-$ YFP^+). First, we tested vaccination with $OVA_{257-264}$-SLP in a prime-boost-boost setting, and this resulted in vaccine-specific $CD8^+$ T cell responses that are comparable to other SLPs with respect to the kinetics and magnitude of the response (**Figure 5A**) as well as the induction of the $KLRG1^+CD62L^-$ phenotype after the first booster vaccination (**Figure 5B**), which further corroborates that vaccine-specific conditions drive the differentiation of elicited $CD8^+$ T cells.

Next, we adoptively transferred the OT-I $CD8^+$ T cells of the Hobit LT mice into naïve wild-type mice that received subsequent $OVA_{257-264}$-SLP vaccinations in a prime-boost-boost setting. As expected, an increase of $CD8^+$ T_{RM} cells ($CD69^+$ $tdTomato^+$ YFP^+) was observed in the liver after the 2nd and 3th vaccination, which were all co-expressing CD38 (**Figure 5C, 5D)**. Remarkably, in particular the 3rd vaccination induced the emergence of ex-T_{RM} cells in the liver, spleen and blood circulation, and the formation of these cells was characterized by the $KLRG1^+CD44^+$ phenotype (**Figure 5D-G**). Thus, ex-T_{RM} cells with a $KLRG1^+$ T_{EM} phenotype are induced upon sequential SLP vaccination and are present in the blood circulation, spleen and liver.

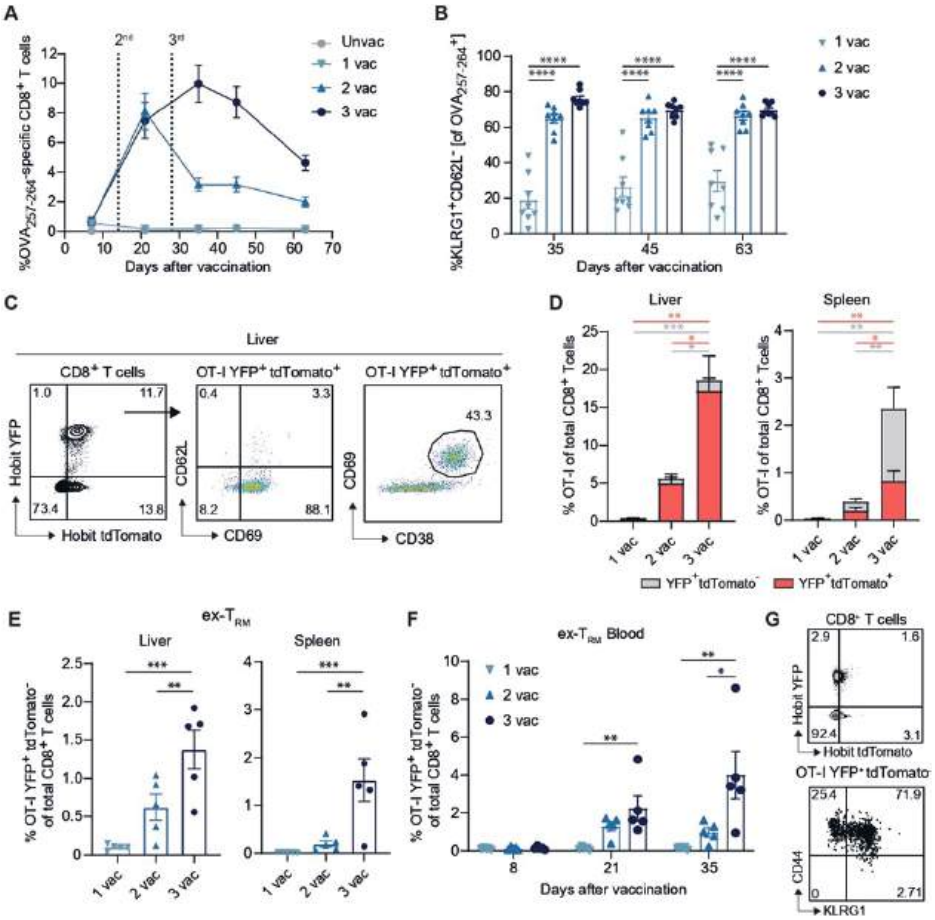

Figure 5. A third vaccination triggers the remigration of T_{RM} cells into the circulation. (A) C57BL/6 mice were vaccinated with the $OVA_{257-264}$ T cell SLP vaccine adjuvanted with CpG in a prime-boost-boost regimen with 2 week intervals. Shown are the $OVA_{257-264}$-specific $CD8^+$ T cell kinetics in blood at indicated days after vaccination. Data is represented as mean ± SEM. **(B)** Frequencies of $KLRG1^+CD62L^-$ $OVA_{257-264}$-specific $CD8^+$ T cells in blood in time. Data is represented as mean ± SEM. Symbols represent individual mice. Two-way ANOVA with repeated measurements was performed to determine significance (n=8). **(C-G)** 1×10^4 OT-I Hobit LT $CD8^+$ T cells were adoptively transferred into C57BL/6 mice. The day after, mice received the first $OVA_{257-264}$-SLP vaccination, followed by 2 boosters. After 50 days spleen and liver were analyzed by flow cytometry. **(C)** Flow cytometry plots showing the CD62L, CD69 and CD38 expression of liver OT-I YFP^+ $tdTomato^+$ $CD8^+$ T cells. **(D)** Percentage of OT-I YFP and/or tdTomato positive $CD8^+$ T cells in liver and spleen. Data is represented as mean ± SEM. One-way ANOVA with repeated measurements was used to determine statistical significance (n=5). **(E)** Percentage of OT-I $tdTomato^+YFP^+$ (ex-T_{RM}) of total $CD8^+$ T cells in liver and spleen. Data is represented as mean ± SEM. Symbols represent individual mice. One-way ANOVA with repeated measurements was used to determine statistical significance (n=5). **(F)** Percentage of OT-I Hobit $tdTomato^+YFP^+$ (ex-T_{RM}) cells of total $CD8^+$ T cells in blood. Data is represented as mean ± SEM. Symbols represent individual mice. One-way ANOVA with repeated measurements was used to determine statistical significance (n=5). **(G)** Phenotype of OT-I $Tomato^-YFP^-$ (ex-T_{RM}) $CD8^+$ T cells in the spleen. One-way ANOVA with repeated measurements was used to determine statistical significance. *P<0.05, **P<0.01, ***P<0.001, ****P<0.0001.

DISCUSSION

Here, we have investigated the capacity of single B cell and T cell epitope-containing peptide vaccines to elicit protection against SARS-CoV-2 infection in the K18-hACE2 transgenic mouse model, and found that only a third vaccination with a long peptide harboring a single T cell epitope provided full protection. To our knowledge this is the first study to show that vaccine-elicited $CD8^+$ T-cells without the aid of virus-specific $CD4^+$ helper T cells or neutralizing antibodies can protect against SARS-CoV-2, albeit provided in a booster setting requiring at least 2 boosters. These results may be of interest for the current discussion regarding a third vaccination, as the current vaccines elicit virus-specific T cells (4). In addition, these results may also guide the development of T-cell focused vaccines, which could be of utmost importance for susceptible patient groups such as transplantation and leukemia patients, and patients with auto-immune diseases treated with anti-CD20 antibodies such as rituximab. These patients have impaired antibody responses, and therefore may depend on robust T cell-eliciting vaccines for protection.

The DNA vaccine platform we used encoding Spike protein was highly efficient in generating neutralizing antibodies and resulted in protection against SARS-CoV-2 infection. Although, our results indicated that antibody responses to single linear B cell epitopes are inferior for induction of neutralizing antibodies, we cannot exclude the possibility that single linear B cell epitopes exist that can elicit neutralizing antibodies. In addition, in settings in which antibodies mediate protection by other mechanisms, such as antibody-dependent cellular cytotoxicity (ADCC), antibody-dependent cellular phagocytosis (ADCP), and complement dependent cytotoxicity (CDC) (33), the B cell-SLP platform may be valuable. In this respect, the addition of CpG and IFA as adjuvants and the insertion of a $CD4^+$ T helper cell epitope to the linear B cell epitope vaccine was indispensable to elicit antibody responses.

In-depth studies using the T cell epitope SLP vaccines indicated that a third vaccination resulted in superior generation of $CD8^+$ T_{EM} cells, as exemplified by the expression of KLRG1, Ly6C and the chemokine receptors CXCR3 and CXRCR1, in the circulation and also of $CD8^+$ T_{RM} cells in liver and lungs. The $CD8^+$ T cells elicited upon a third dose vaccination are functionally and phenotypically modulated as evidenced by activation-associated cell-surface markers and their polyfunctional cytokine production. The latter is in line with a recent study in humans, which indicated that a third vaccination in kidney transplant recipients leads to increased circulating polyfunctional $CD4^+$ T cells (34). It would be of interest to decipher whether a third dose of the mRNA vaccine in healthy individuals, which is more effective against severe COVID-19-related outcomes

compared to two doses (35), also associates to increased T cell immunity. It is also of interest to examine whether differential time-intervals between the prime and booster vaccinations have impact on the magnitude and phenotype of the vaccine-elicited T cells (36, 37). A recent study indicated only differences for the induction of IL-2-expressing $CD4^+$ T cell responses by mRNA vaccines when comparing intervals of 3-6 weeks to 8-16 weeks between the first and second dose but shorter intervals were not compared (37). Strikingly, the phenotype and cytokine polyfunctionality was highly similar between the different SLP vaccines, indicating that vaccine-specific conditions are dominant in shaping the T cell phenotype rather than the epitope used. This is in line with other studies showing that the environmental cues during T cell activation dictate the differentiation of these cells (31, 38, 39).

The increase of T_{EM} and T_{RM} cells in the lungs after the third vaccination as reported here may be critical as the lungs are the primary entry point for SARS-CoV-2. Nevertheless, the circulating vaccine-induced T cells in the spleen and blood may also contribute to protection as well as these cells can rapidly migrate into the infected lung tissue and exert effector function. Moreover, also the efficient formation of the T_{RM} cells in the liver, which was mainly observed after the third vaccination, may contribute to protection as these cells have superior potential to differentiate into ex-T_{RM} cells (40).

In conclusion, a third vaccination with a synthetic vaccine containing a single $CD8^+$ T cell epitope results in protection against SARS-CoV-2 in the absence or neutralizing antibodies. This protection can be explained by an improved quantitative and qualitative $CD8^+$ T cell response after the third vaccination that is highlighted by higher numbers of virus-specific T_{EM} and T_{RM} cells with polyfunctional cytokine capacity.

REFERENCES

1. Polack FP, Thomas SJ, Kitchin N, Absalon J, Gurtman A, Lockhart S, et al. Safety and Efficacy of the BNT162b2 mRNA Covid-19 Vaccine. N Engl J Med. 2020;383(27):2603-15.
2. Baden LR, El Sahly HM, Essink B, Kotloff K, Frey S, Novak R, et al. Efficacy and Safety of the mRNA-1273 SARS-CoV-2 Vaccine. N Engl J Med. 2021;384(5):403-16.
3. Chia WN, Zhu F, Ong SWX, Young BE, Fong SW, Le Bert N, et al. Dynamics of SARS-CoV-2 neutralising antibody responses and duration of immunity: a longitudinal study. Lancet Microbe. 2021;2(6):e240-e9.
4. Sattler A, Schrezenmeier E, Weber UA, Potekhin A, Bachmann F, Straub-Hohenbleicher H, et al. Impaired humoral and cellular immunity after SARS-CoV-2 BNT162b2 (tozinameran) prime-boost vaccination in kidney transplant recipients. J Clin Invest. 2021;131(14).
5. Wadei HM, Gonwa TA, Leoni JC, Shah SZ, Aslam N, Speicher LL. COVID-19 infection in solid organ transplant recipients after SARS-CoV-2 vaccination. Am J Transplant. 2021;21(10):3496-9.
6. Herishanu Y, Avivi I, Aharon A, Shefer G, Levi S, Bronstein Y, et al. Efficacy of the BNT162b2 mRNA COVID-19 vaccine in patients with chronic lymphocytic leukemia. Blood. 2021;137(23):3165-73.
7. Planas D, Veyer D, Baidaliuk A, Staropoli I, Guivel-Benhassine F, Rajah MM, et al. Reduced sensitivity of SARS-CoV-2 variant Delta to antibody neutralization. Nature. 2021;596(7871):276-80.
8. Garcia-Beltran WF, Lam EC, St Denis K, Nitido AD, Garcia ZH, Hauser BM, et al. Multiple SARS-CoV-2 variants escape neutralization by vaccine-induced humoral immunity. Cell. 2021;184(9):2372-83.e9.
9. Noh JY, Jeong HW, Kim JH, Shin EC. T cell-oriented strategies for controlling the COVID-19 pandemic. Nat Rev Immunol. 2021:1-2.
10. Heitmann JS, Bilich T, Tandler C, Nelde A, Maringer Y, Marconato M, et al. A COVID-19 peptide vaccine for the induction of SARS-CoV-2 T cell immunity. Nature. 2021.
11. Rydyznski Moderbacher C, Ramirez SI, Dan JM, Grifoni A, Hastie KM, Weiskopf D, et al. Antigen-Specific Adaptive Immunity to SARS-CoV-2 in Acute COVID-19 and Associations with Age and Disease Severity. Cell. 2020;183(4):996-1012.e19.
12. Mallajosyula V, Ganjavi C, Chakraborty S, McSween AM, Pavlovitch-Bedzyk AJ, Wilhelmy J, et al. CD8(+) T cells specific for conserved coronavirus epitopes correlate with milder disease in COVID-19 patients. Sci Immunol. 2021;6(61).
13. Bange EM, Han NA, Wileyto P, Kim JY, Gouma S, Robinson J, et al. CD8(+) T cells contribute to survival in patients with COVID-19 and hematologic cancer. Nat Med. 2021;27(7):1280-9.
14. Le Bert N, Tan AT, Kunasegaran K, Tham CYL, Hafezi M, Chia A, et al. SARS-CoV-2-specific T cell immunity in cases of COVID-19 and SARS, and uninfected controls. Nature. 2020;584(7821):457-62.
15. Tan AT, Linster M, Tan CW, Le Bert N, Chia WN, Kunasegaran K, et al. Early induction of functional SARS-CoV-2-specific T cells associates with rapid viral clearance and mild disease in COVID-19 patients. Cell Rep. 2021;34(6):108728.
16. Braun J, Loyal L, Frentsch M, Wendisch D, Georg P, Kurth F, et al. SARS-CoV-2-reactive T cells in healthy donors and patients with COVID-19. Nature. 2020;587(7833):270-4.
17. Zhuang Z, Lai X, Sun J, Chen Z, Zhang Z, Dai J, et al. Mapping and role of T cell response in SARS-CoV-2-infected mice. J Exp Med. 2021;218(4).
18. McMahan K, Yu J, Mercado NB, Loos C, Tostanoski LH, Chandrashekar A, et al. Correlates of protection against SARS-CoV-2 in rhesus macaques. Nature. 2021;590(7847):630-4.
19. Zhao J, Zhao J, Perlman S. T cell responses are required for protection from clinical disease and for virus clearance in severe acute respiratory syndrome coronavirus-infected mice. J Virol. 2010;84(18):9318-25.

20. Zhao J, Zhao J, Mangalam AK, Channappanavar R, Fett C, Meyerholz DK, et al. Airway Memory CD4(+) T Cells Mediate Protective Immunity against Emerging Respiratory Coronaviruses. Immunity. 2016;44(6):1379-91.
21. van der Gracht ET, Schoonderwoerd MJ, van Duikeren S, Yilmaz AN, Behr FM, Colston JM, et al. Adenoviral vaccines promote protective tissue-resident memory T cell populations against cancer. J Immunother Cancer. 2020;8(2).
22. Beyrend G, van der Gracht E, Yilmaz A, van Duikeren S, Camps M, Hollt T, et al. PD-L1 blockade engages tumor-infiltrating lymphocytes to co-express targetable activating and inhibitory receptors. J Immunother Cancer. 2019;7(1):217.
23. Bartholdy C, Stryhn A, Christensen JP, Thomsen AR. Single-epitope DNA vaccination prevents exhaustion and facilitates a broad antiviral CD8+ T cell response during chronic viral infection. J Immunol. 2004;173(10):6284-93.
24. Xu HB, Xu W, Chu YW, Wang Y, Xiong S. Single B or T-cell epitope-based DNA vaccine using modified vector induces specific immune response against hepadnavirus. Immunol Lett. 2005;99(2):186-92.
25. Poh CM, Carissimo G, Wang B, Amrun SN, Lee CY, Chee RS, et al. Two linear epitopes on the SARS-CoV-2 spike protein that elicit neutralising antibodies in COVID-19 patients. Nat Commun. 2020;11(1):2806.
26. Amrun SN, Lee CY, Lee B, Fong SW, Young BE, Chee RS, et al. Linear B-cell epitopes in the spike and nucleocapsid proteins as markers of SARS-CoV-2 exposure and disease severity. EBioMedicine. 2020;58:102911.
27. Yoshida S, Ono C, Hayashi H, Fukumoto S, Shiraishi S, Tomono K, et al. SARS-CoV-2-induced humoral immunity through B cell epitope analysis in COVID-19 infected individuals. Sci Rep. 2021;11(1):5934.
28. Winkler ES, Bailey AL, Kafai NM, Nair S, McCune BT, Yu J, et al. SARS-CoV-2 infection of human ACE2-transgenic mice causes severe lung inflammation and impaired function. Nat Immunol. 2020;21(11):1327-35.
29. Zhi Y, Kobinger GP, Jordan H, Suchma K, Weiss SR, Shen H, et al. Identification of murine CD8 T cell epitopes in codon-optimized SARS-associated coronavirus spike protein. Virology. 2005;335(1):34-45.
30. Bendall SC, Davis KL, Amir el AD, Tadmor MD, Simonds EF, Chen TJ, et al. Single-cell trajectory detection uncovers progression and regulatory coordination in human B cell development. Cell. 2014;157(3):714-25.
31. van der Gracht ETI, Beyrend G, Abdelaal T, Pardieck IN, Wesselink TH, van Haften FJ, et al. Memory CD8+ T cell heterogeneity is primarily driven by pathogen-specific cues and additionally shaped by the tissue environment. iScience. 2021;24(1):101954.
32. Behr FM, Parga-Vidal L, Kragten NAM, van Dam TJP, Wesselink TH, Sheridan BS, et al. Tissue-resident memory CD8(+) T cells shape local and systemic secondary T cell responses. Nat Immunol. 2020;21(9):1070-81.
33. Sedova ES, Scherbinin DN, Lysenko AA, Alekseeva SV, Artemova EA, Shmarov MM. Non-neutralizing Antibodies Directed at Conservative Influenza Antigens. Acta Naturae. 2019;11(4):22-32.
34. Schrezenmeier E, Rincon-Arevalo H, Stefanski AL, Potekhin A, Staub-Hohenbleicher H, Choi M, et al. B and T Cell Responses after a Third Dose of SARS-CoV-2 Vaccine in Kidney Transplant Recipients. J Am Soc Nephrol. 2021.
35. Barda N, Dagan N, Cohen C, Hernán MA, Lipsitch M, Kohane IS, et al. Effectiveness of a third dose of the BNT162b2 mRNA COVID-19 vaccine for preventing severe outcomes in Israel: an observational study. Lancet. 2021;398(10316):2093-100.
36. Gilfillan CB, Wang C, Mohsen MO, Rufer N, Hebeisen M, Allard M, et al. Murine CD8 T-cell functional avidity is stable in vivo but not in vitro: Independence from homologous prime/boost time interval and antigen density. Eur J Immunol. 2020;50(4):505-14.
37. Hall VG, Ferreira VH, Wood H, Ierullo M, Majchrzak-Kita B, Manguiat K, et al. Delayed-interval BNT162b2 mRNA COVID-19 vaccination enhances humoral immunity and induces robust T cell responses. Nat Immunol. 2022;23(3):380-5.

38. Plumlee CR, Sheridan BS, Cicek BB, Lefrancois L. Environmental cues dictate the fate of individual CD8+ T cells responding to infection. Immunity. 2013;39(2):347-56.
39. Welten SP, Redeker A, Franken KL, Oduro JD, Ossendorp F, Cicin-Sain L, et al. The viral context instructs the redundancy of costimulatory pathways in driving CD8(+) T cell expansion. Elife. 2015;4:e07486.
40. Christo SN, Evrard M, Park SL, Gandolfo LC, Burn TN, Fonseca R, et al. Discrete tissue microenvironments instruct diversity in resident memory T cell function and plasticity. Nat Immunol. 2021;22(9):1140-51.
41. McCray PB, Jr., Pewe L, Wohlford-Lenane C, Hickey M, Manzel L, Shi L, et al. Lethal infection of K18-hACE2 mice infected with severe acute respiratory syndrome coronavirus. J Virol. 2007;81(2):813-21.
42. Arens R, Loewendorf A, Redeker A, Sierro S, Boon L, Klenerman P, et al. Differential B7-CD28 costimulatory requirements for stable and inflationary mouse cytomegalovirus-specific memory CD8 T cell populations. J Immunol. 2011;186(7):3874-81.

SUPPLEMENTARY MATERIALS

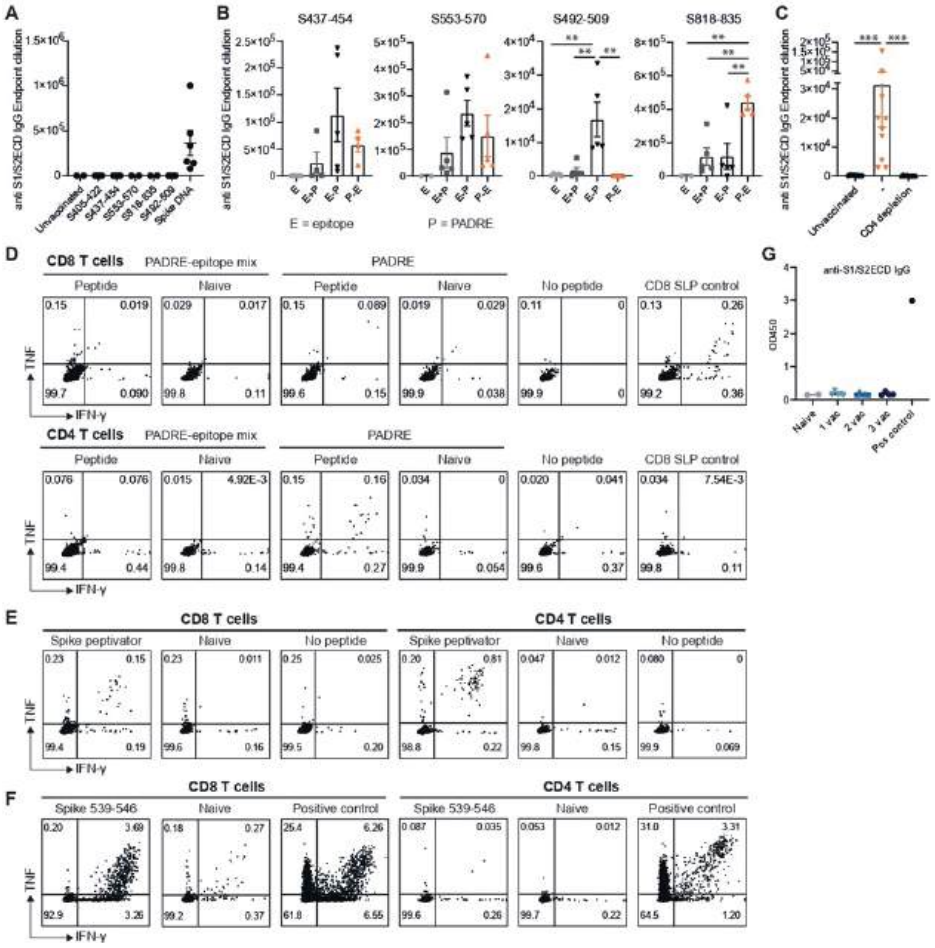

Supplementary Figure 1. Synthetic long peptide (SLP)-based vaccines containing a single B cell epitope require adjuvants to elicit antibodies. (A) C57BL/6 mice were subcutaneously vaccinated on day 0, day 14 and day 28 with SLPs consisting of linear B cell epitopes adjuvanted with CpG and Inactivated Freund's Adjuvant. Spike-specific IgG in blood was determined at day 42 after vaccination. Serum from a Spike-encoding DNA vaccinated animal was used as a positive control. Results are depicted as the endpoint dilution. Data is represented as mean ± SEM. **(B)** C57BL/6 mice were vaccinated as described in (A) with SLPs consisting of PADRE-coupled linear B cell epitopes (E-P) or equimolar controls of the epitope alone (E), or the epitope combined with PADRE (E+P). Spike-specific IgG in blood at day 42 after vaccination. Results are depicted as the endpoint dilution. Data is represented as mean ± SEM. One-way ANOVA with repeated measurements was performed to determine statistical significance (n=2-5). **(C)** Spike-specific IgG antibodies in blood at day 27 in unvaccinated mice and in $CD4^+$ T cell depleted and proficient mice that were vaccinated with SLPs consisting of linear B cell epitopes coupled to PADRE. Results are depicted as the endpoint dilution. Data is represented as mean ± SEM. A Kruskal-Wallis test with multiple comparisons was performed to determine significance (n=10). **(D)** Intracellular cytokine production (IFN-γ and TNF) of $CD8^+$ and $CD4^+$ T cells in the spleen at day 35 after >

> linear B/PADRE SLP vaccination. Splenocytes were stimulated with the linear B cell epitope coupled to PADRE SLPs, PADRE alone or no peptide. **(E)** Intracellular cytokine production (IFN-γ and TNF) of $CD8^+$ and $CD4^+$ T cells in the spleen at day 70 after DNA vaccination. Splenocytes were stimulated with the S1 peptivator mix. **(F)** Intracellular cytokine production of splenic $CD8^+$ and $CD4^+$ T cells at day 35 post vaccination stimulated with $Spike_{539-546}$-SLP. **(G)** OD450 of Spike-specific IgG in blood at day 42 after either 1, 2 or 3 times vaccination with the SARS-CoV-2 $CD8^+$ T cell SLP. Serum from a Spike-encoding DNA vaccinated animal was used as a positive control. Data is represented as mean ± SEM. In all bar graphs, symbols represent individual mice. **P<0.01, ***P<0.001.

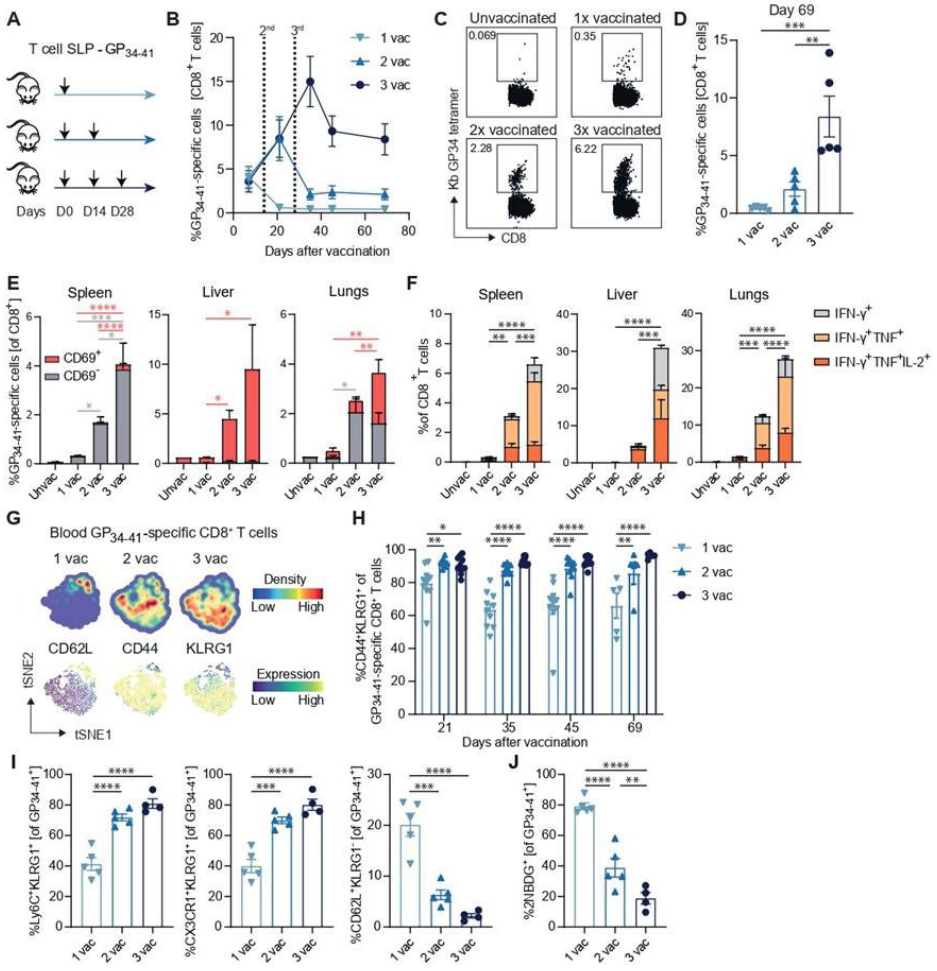

Supplementary Figure 2. A third vaccination with a single T cell epitope augments effector-memory and tissue-resident memory $CD8^+$ T cell formation. (A) C57BL/6 mice were vaccinated with the GP_{34-41}-SLP vaccine adjuvanted with CpG in a prime-boost-boost regimen with 2 week intervals. **(B)** GP_{34-41}-specific $CD8^+$ T cell kinetics in blood at indicated days after vaccination. Data is represented as mean ± SEM. **(C)** Representative flow cytometry plots of GP_{34-41}-specific $CD8^+$ T cells determined by MHC class I tetramer staining. **(D)** GP_{34-41}-specific $CD8^+$ T cells in blood at day 69 after vaccination. Bar graphs represent means ± SEM. Symbols represent individual mice. One-way ANOVA with repeated >

> measurements was performed to determine statistical significance (n=5). **(E)** Frequencies of $CD69^+$ and $CD69^-$ GP_{34-41}-specific $CD8^+$ T cells in the $CD8^+$ T cell population in the spleen, liver and lungs at day 66 after 1, 2 or 3 vaccinations. Bar graphs represent mean ± SEM. One-way ANOVA with repeated measurements was performed to determine statistical significance (n=9-10). **(F)** Intracellular cytokine production of $CD8^+$ T cells upon stimulation with the GP_{34-41} peptide epitope in different tissues on day 66 after SLP vaccination. Data is represented as mean ± SEM (n=4-10). **(G)** tSNE maps describing the local probability density of GP_{34-41}-specific $CD8^+$ T cells in the blood stained for CD62L, CD44, KLRG1 at day 71 after 1, 2 and 3 vaccinations. **(H)** Frequencies of $CD44^+KLRG1^+$ GP_{34-41}-specific $CD8^+$ T cells in blood at indicated time points. Data is represented as mean ± SEM. A two-way ANOVA with repeated measurements was performed to determine statistical significance (n=5-10). **(I)** Cell surface marker ($Ly6C^+KLRG1^+$, $CX3CR1^+KLRG1^+$ and $CD62L^+KLRG1^-$) expression on GP_{34-41}-specific $CD8^+$ T cells at day 66 in spleen after 1, 2 or 3 vaccinations. Data is represented as mean ± SEM and is representative data of two independent experiments. Symbols represent individual mice. **(J)** Glucose analog 2-(N-(7-nitrobenz-2-oxa-1,3-diazol-4-yl)amino)-2-deoxyglucose (2NBDG) uptake of splenic GP_{34-41}-specific $CD8^+$ T cells at day 66 after 1, 2 and 3 vaccinations. Symbols represent individual mice. One-way ANOVA with repeated measurements was performed to determine statistical significance (n=5). *P<0.05, **P<0.01, ***P<0.001, ****P<0.0001.

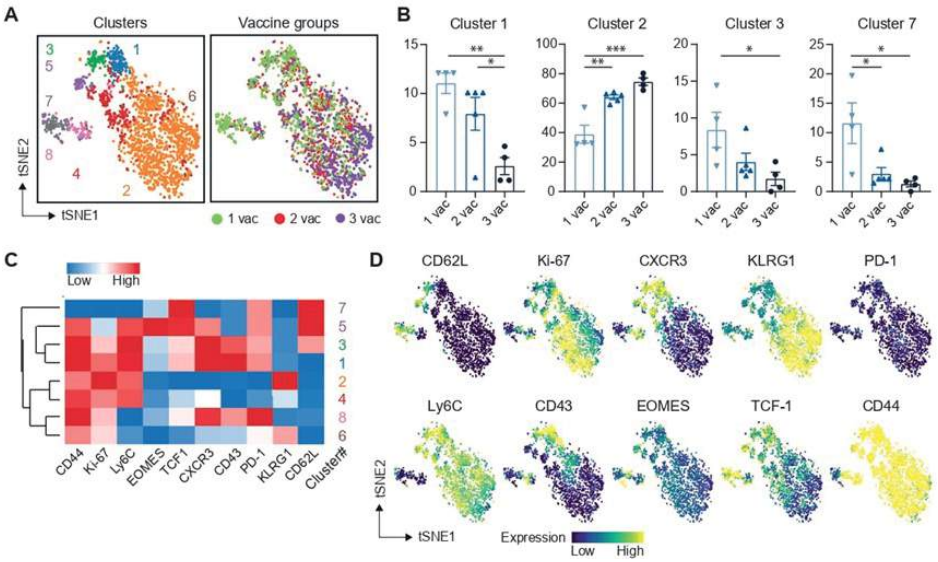

Supplementary Figure 3. Progressive differentiation of vaccine-specific $CD8^+$ T cells after booster vaccination. C57BL/6 mice were vaccinated subcutaneously on day 0 (1st vaccination), day 14 (2nd vaccination) and day 28 (3rd vaccination) with the GP_{34-41}-SLP vaccine adjuvanted with CpG and sacrificed on day 66. Following tSNE analysis and downsampling, FlowSOM consensus metaclustering with 8 clusters was performed on 695 live $CD3^+CD8^+CD4^-CD19^-$ GP_{34-41} tetramer$^+$ cells per group. Overlay of **(A)** the 8 FlowSOM clusters and vaccination status on the tSNE-map. **(B)** Significant clusters were selected and shown in bar graphs. Data is represented as mean ± SEM. Symbols represent individual mice. One-way ANOVA with repeated measurements was performed to determine statistical significance (n=4-5). **(C)** Hierarchically clustered heatmap of phenotypes of the clusters shown in (A) – the indicated marker expression is shown per cluster as z-Score of median signal intensity per channel; blue, low expression; red, high expression. **(D)** Expression intensity of cell surface markers (color indication: blue, low expression; yellow, high expression). *P<0.05, **P<0.01, ***P<0.001, ****P<0.0001.

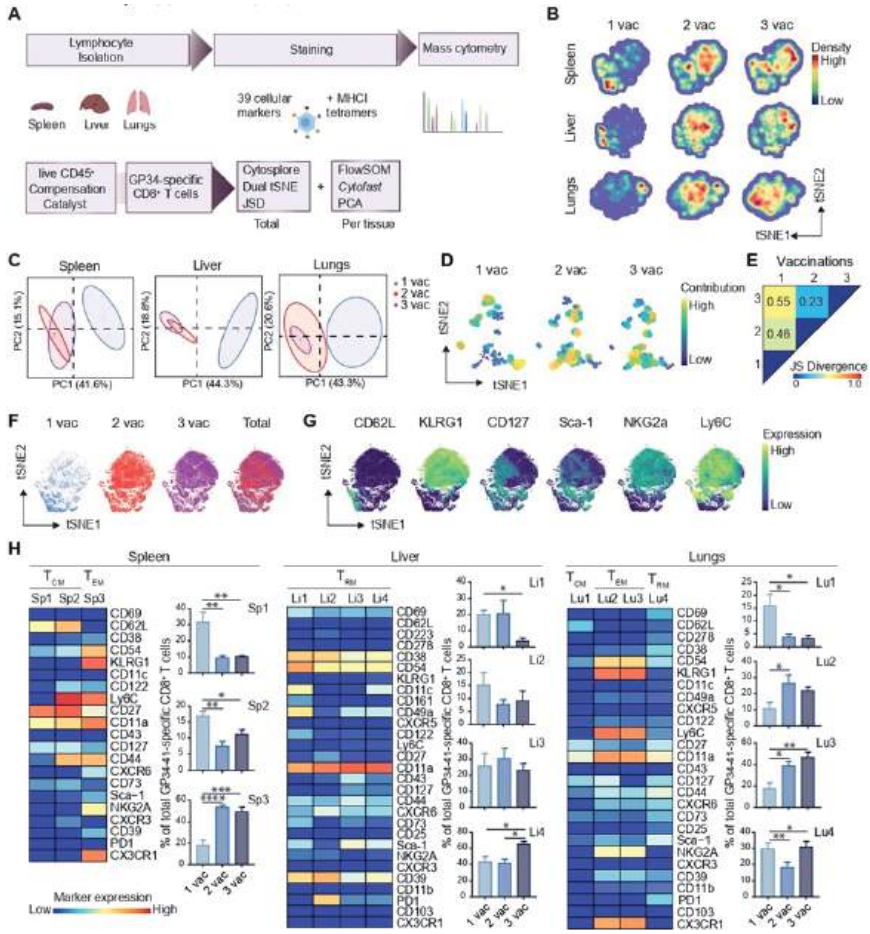

Supplementary Figure 4. Booster vaccination impacts the differentiation of vaccine-specific CD8⁺ T cells system-wide. (A) Schematic of the mass cytometric analysis of lymphocytes isolated from spleen, liver, and lungs. **(B)** tSNE maps describing the local probability density of GP_{34-41}-specific $CD8^+$ T cells in spleen, liver and lungs stained at day 71 after 1, 2 and 3 vaccinations with the mass cytometry panel. **(C)** Principal Component Analysis illustrating the phenotypic dissimilarity of GP_{34-41}-specific $CD8^+$ T cells per tissue upon multiple vaccinations. **(D)** tSNE maps showing GP_{34-41}-specific $CD8^+$ T cell clusters per vaccination. Clusters with similar composition profiles across samples end up close together in the map. The varying dot size and color in this cluster tSNE map shows the average cluster normalized frequencies per vaccination group. **(E)** Pairwise Jensen-Shannon Divergence plots of the tSNE map obtained from all samples of GP_{34-41}-specific $CD8^+$ T cells grouped by vaccinations. **(F)** tSNE embedding of GP_{34-41}-specific $CD8^+$ T cells isolated from vaccinated mice and multiple tissues in one analysis. Cells are color coded per vaccination. **(G)** Expression intensity of the cell-surface markers on the GP_{34-41}-specific $CD8^+$ T cells. The color of the cells indicates ArcSinh5-transformed expression values for a given marker analyzed. **(H)** Heat maps of GP_{34-41}-specific $CD8^+$ T cell clusters in the spleen, liver and lungs of mice that received multiple vaccinations. Clusters were selected based on their significant difference and categorized in T_{CM}, T_{EM} and T_{RM} subsets. Bar graphs indicate the average percentage (± SEM) of each $CD8^+$ T cell cluster within the GP_{34-41}-specific $CD8^+$ T -cell population elicited by one, two and three vaccinations. One-way ANOVA with repeated measurements was performed to determine statistical significance (n=5). *P<0.05, **P<0.01, ***P<0.001, ****P<0.0001.

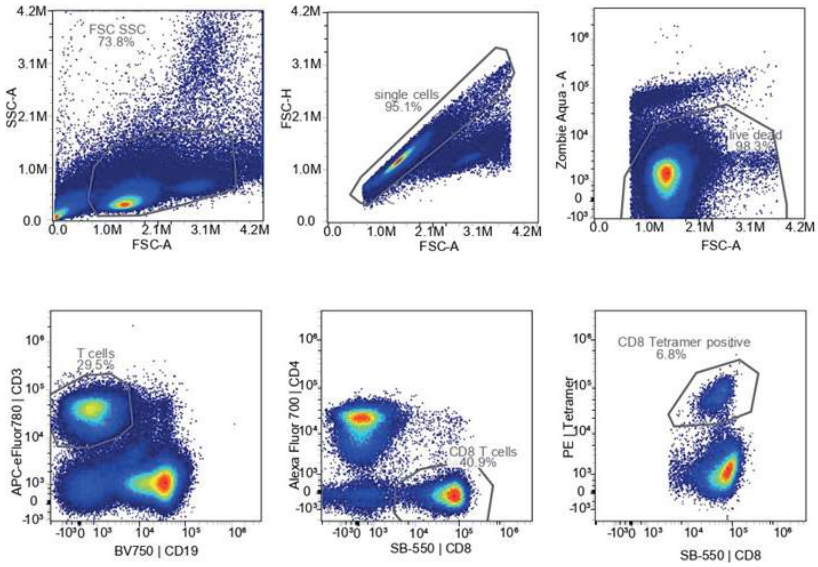

Supplementary Figure 5. Flow cytometry gating strategies. Representative plots show the gating strategy for detecting MHC class I tetramer positive cells depicted. In this sequential gating, cells were first gated on lymphocytes (forward-scatter (FSC-A) vs. side-scatter (SSC-A)) and then on singlets (FSC-A vs. FSC-H). The cells were next analysed for their uptake of Zombie Aqua to exclude dead cells, and followed by their expression of CD3 and CD8. Finally, MHC class I tetramer positive cells were gated on the live $CD3^{+}CD8^{+}$ T cell population.

Supplementary Table 1. CyTOF Mass Cytometry Panel.

Antibody	Clone	Metal	Pre-conjugated	Company	Cat no	Cat no metal (Fluidigm)
Anti-PE	PE001	165 Ho	x	Fluidigm	3165015B	
Anti-APC	APC003	176 Yb	x	Fluidigm	3176007B	
CD3e	145-2C11	172 Yb		eBioscience	14-0031-86	201172A
CD4	RM4-5	145 Nd	x	Fluidigm	3145002B	
CD8a	53-6.7	168 Er	x	Fluidigm	3168003B	
CD8b	YTS156.7.7	194 Pt		BioLegend	126602	201194
CD11a	M17/4	160 Gd		eBioscience	16-0111-82	201160A
CD11b	M1/70	154 Sm	x	Fluidigm	3154006B	
CD11c	N418	167 Er		eBioscience	14-0114-85	201167A
CD19	6D5	Qdot655: 112/114 Cd	x	ThermoFisher	Q10379	
CD25	3C7	150 Nd	x	Fluidigm	3150002B	
CD27	LG.3A10	158 Gd		eBioscience	14-0272-82	201158A
CD38	90	163 Dy		eBioscience	14-0381-85	201163A
CD39	24DMS1	152 Sm		eBioscience	14-0391-82	201152A
CD43	1B11	115 In		BioLegend	121202	
CD44	IM7	142 Nd		eBioscience	14-0441-86	201142A
CD45	30-F11	89Y	x	Fluidigm	3089005B	
CD49a	Ha31/8	151 Eu		BD Biosciences	555001	201151A
CD54	YN1/1.7.4	164 Dy		BioLegend	116102	201164A
CD62L	MEL-14	169 Tm		BioLegend	104443	201169A
CD69	H1.2F3	143 Nd	x	Fluidigm	3143004B	
CD73	TY/23	148 Nd		BD Biosciences	550738	201148A
CD86	GL1	171 Yb		eBioscience	14-0862-85	201171A
CD103	2.E7	173 Yb		eBioscience	14-1031-85	201173A
CD122	TM-b1	155 Gd		eBioscience	14-1222-85	201155A
CD127	A7R34	175 Lu	x	Fluidigm	3175006B	
CD160	7H1	209 Bi		BioLegend	143002	
CD161	PK136	170 Er	x	Fluidigm	3170002B	
CD223	eBioC9B7W	161 Dy		eBioscience	14-2231-85	201161A
CD278	7E.17G9	162 Dy		eBioscience	14-9942-85	201162A
CX3CR1	SA011F11	174 Yb		BioLegend	149002	201174A
CXCR3	CXCR3-173	149 Sm		eBioscience	16-1831-85	201149A
CXCR5	L138D7	153 Eu		BioLegend	145502	201153A
CXCR6	SA051D1	144 Nd		BioLegend	151102	201144A

Supplementary Table 1. Continued.

Antibody	Clone	Metal	Pre-conjugated	Company	Cat no	Cat no metal (Fluidigm)
FR4	TH6	198 Pt		BioLegend	125102	201198
KLRG1	2F1	166 Er		eBioscience	16-5893-85	201166A
Ly6C	HK1.4	156 Gd		eBioscience	16-5932-85	201156A
NKG2A	20d5	147 Sm		eBioscience	16-5896-85	201147A
PD-1	29F.1A12	159 Tb	x	Fluidigm	3159024B	
Sca-1	D7	141 Pr		BioLegend	108135	201141A
TCRgd	eBioGL3	146 Nd		eBioscience	14-5711-85	201146A

Anti-mouse monoclonal antibodies used for staining of cells for mass cytometry analysis. Antibodies were either purchased pre-conjugated, or antibodies were conjugated to the indicated lanthanide metal isotopes.

Supplementary Table 2. Linear B cell epitope peptides

PADRE	AKXVAAWTLKAuB
$Spike_{553-570}$	TESNKKFLPFQQFGRDIA
$Spike_{553-570}$-PADRE	TESNKKFLPFQQFGRDIAAKXVAAWTLKAuB
PADRE-$Spike_{553-570}$	AKXVAAWTLKAuTESNKKFLPFQQFGRDIA
$Spike_{818-835}$	PSKPSKRSFIEDLLFNKV
$Spike_{818-835}$-PADRE	PSKPSKRSFIEDLLFNKVAKXVAAWTLKAuB
PADRE-$Spike_{818-835}$	AKXVAAWTLKAuPSKPSKRSFIEDLLFNKV
$Spike_{405-422}$	DEVRQIAPGQTGKIADYN
$Spike_{405-422}$-PADRE	DEVRQIAPGQTGKIADYNAKXVAAWTLKAuB
PADRE-$Spike_{405-422}$	AKXVAAWTLKAuDEVRQIAPGQTGKIADYN
$Spike_{437-454}$	NSNNLDSKVGGNYNYLYR
$Spike_{437-454}$-PADRE	NSNNLDSKVGGNYNYLYRAKXVAAWTLKAuB
PADRE-$Spike_{437-454}$	AKXVAAWTLKAuNSNNLDSKVGGNYNYLYR
$Spike_{492-509}$	LQSYGFQPTNGVGYQPYR
$Spike_{492-509}$-PADRE	LQSYGFQPTNGVGYQPYRAKXVAAWTLKAuB
PADRE-$Spike_{492-509}$	AKXVAAWTLKAuLQSYGFQPTNGVGYQPYR
$Spike_{539-546}$	IKNQCVNFNFNGLTGTGVLTESNK
GP_{34-41}	KAVYNFATCGIFALIS
OVA	SMLVLLPDEVSGLEQLESIINFEKLTEWTS

X = cyclohexylalanine, u = d-Ala, B = amide

SUPPLEMENTARY METHOD

Mass cytometry and analysis. Metal-conjugated antibodies were either purchased from Fluidigm or were generated by conjugation of lanthanide metal isotopes to anti-mouse antibodies using the Maxpar X8 Polymer method according to the manufacturer's protocol (Fluidigm). Cisplatins 194 and 198 and Bismuth 209 were conjugated to anti-mouse monoclonal antibodies using protocols previously described (1, 2). All in-house conjugated antibodies were diluted to 0.5 mg/ml in antibody stabilizer supplemented with 0.05% sodium azide (Candor Biosciences). Serial dilution staining was performed on mouse lymphocytes to determine appropriate antibody dilution.

The CyTOF staining was performed as described elsewhere (3). In brief, around 3×10^6 cells per sample were stained for CyTOF analysis. First, cells were stained in FACS buffer with PE and APC labelled tetramers and incubated for 30 minutes on ice. Cells were washed with Maxpar Cell Staining buffer (201068, Fluidigm) and subsequently incubated for 20 minutes with 1 µM Interchalator-Rh (201103A, Fluidigm) in staining buffer. Next, aspecific binding was prevented by incubating cells with Fc blocking solution and mouse serum for 15 minutes. Anti-PE and anti-APC were added and incubated for 45 minutes. The antibody mix was added and incubated for an additional 45 minutes. After washing the cells, samples were incubated overnight with 25nM Intercalator-Ir (201192A, Fluidigm) in Maxpar Fix and Perm Buffer (201067, Fluidigm). Cells were pelleted in staining buffer and measured within one week. Before measuring, EQ™ Four Element Calibration Beads (201078, Fluidigm) were added in a 1:10 ratio. Mass cytometry data analysis focused on the antigen-specific $CD8^+$ T cells. For the selection, we set our gating strategy to live single cells, positive for CD45, and excluded reference beads. The live $CD45^+$ gated files were compensated using Catalyst (4). Subsequently, MHC class I tetramer-specific $CD8^+$ T cells were selected in FlowJo for subsequent analysis. Next, marker expression was ArcSinh5 transformed and subjected to dimensionality reduction analyses and cluster identification using Cytosplore (5) or FlowSOM (6). For Cytosplore analysis, samples were analysed by hierarchical stochastic neighbor embedding (HSNE) (7) based on approximated t-distributed stochastic neighbor embedding (A-tSNE) (8). The similarity between tSNE maps was quantified using the Jensen-Shannon (JS) divergence as previously described (3). The JS divergence values ranged from 0 (indicating identical distributions) to 1 (indicating disjoint distributions). The dual tSNE analysis was performed to quantify the individual samples similarity based on the clusters composition as previously described (3, 9). FlowSOM was used for the identification of vaccination and tissue-specific clusters. Using FlowSOM, 14 clusters were identified per analysis. Subsequently, Cytofast (10, 11) was used for visualization and quantification of cell clusters. T_{RM} ($CD62L^-$ $CD69^+$), T_{CM} ($CD62L^+$ $CD69^-$) and T_{EM}

(CD62L^{-}CD69^{-}) CD8^{+} T cell clusters were selected by expression of CD62L and CD69. Visualization of heatmaps and selection of clusters based on the size of the cluster (abundance of at least >5% of total) and significance was performed as previously described (3).

SUPPLEMENTARY REFERENCES

1. Mei HE, Leipold MD, Maecker HT. Platinum-conjugated antibodies for application in mass cytometry. Cytometry A. 2016;89(3):292-300.
2. Spitzer MH, Carmi Y, Reticker-Flynn NE, Kwek SS, Madhireddy D, Martins MM, et al. Systemic Immunity Is Required for Effective Cancer Immunotherapy. Cell. 2017;168(3):487-502.e15.
3. van der Gracht ETI, Beyrend G, Abdelaal T, Pardieck IN, Wesselink TH, van Haften FJ, et al. Memory CD8+ T cell heterogeneity is primarily driven by pathogen-specific cues and additionally shaped by the tissue environment. iScience. 2021;24(1):101954.
4. Chevrier S, Crowell HL, Zanotelli VRT, Engler S, Robinson MD, Bodenmiller B. Compensation of Signal Spillover in Suspension and Imaging Mass Cytometry. Cell Systems. 2018;6(5):612-20.e5.
5. Höllt T, Pezzotti N, van Unen V, Koning F, Eisemann E, Lelieveldt B, et al. Cytosplore: Interactive Immune Cell Phenotyping for Large Single-Cell Datasets. Computer Graphics Forum. 2016;35(3):171-80.
6. Van Gassen S, Callebaut B, Van Helden MJ, Lambrecht BN, Demeester P, Dhaene T, et al. FlowSOM: Using self-organizing maps for visualization and interpretation of cytometry data. Cytometry A. 2015;87(7):636-45.
7. van Unen V, Höllt T, Pezzotti N, Li N, Reinders MJT, Eisemann E, et al. Visual analysis of mass cytometry data by hierarchical stochastic neighbour embedding reveals rare cell types. Nature Communications. 2017;8(1):1740.
8. Pezzotti N, Lelieveldt BPF, Van Der Maaten L, Hollt T, Eisemann E, Vilanova A. Approximated and User Steerable tSNE for Progressive Visual Analytics. IEEE Trans Vis Comput Graph. 2017;23(7):1739-52.
9. van Unen V, Li N, Molendijk I, Temurhan M, Hollt T, van der Meulen-de Jong AE, et al. Mass Cytometry of the Human Mucosal Immune System Identifies Tissue- and Disease-Associated Immune Subsets. Immunity. 2016;44(5):1227-39.
10. Beyrend G, Stam K, Hollt T, Ossendorp F, Arens R. Cytofast: A workflow for visual and quantitative analysis of flow and mass cytometry data to discover immune signatures and correlations. Comput Struct Biotechnol J. 2018;16:435-42.
11. Beyrend G, Stam K, Ossendorp F, Arens R. Visualization and Quantification of High-Dimensional Cytometry Data using Cytofast and the Upstream Clustering Methods FlowSOM and Cytosplore. J Vis Exp. 2019(154).